Proportionality between ion-beam-induced epitaxial regrowth in silicon and nuclear energy deposition

J. Linnros, G. Holmén, and B. Svensson*
Department of Physics, Chalmers University of Technology, S-412 96 Göteborg, Sweden
(Received 28 January 1985)

Amorphous surface layers in silicon on sapphire have been epitaxially regrown with the use of ion beams. The amorphous layers, 1600 Å thick, were formed by ion implantation of 2×10^{15} $^{28}Si^+$ ions/cm^2 of 80 keV energy at room temperature. The subsequent ion-beam-induced annealing was performed at a target temperature of 300 °C with low-intensity beams of He^+, N^+, Ne^+, Si^+, Ar^+, and Kr^+ ions of 300 keV energy. Rutherford-backscattering and channeling technique with 315-keV protons was used for the analysis of the epitaxial regrowth. It is shown that the initial regrowth rate is proportional to the amount of energy deposited in elastic collisions by the annealing ions near the amorphous-crystalline interface. Support is given for a model in which migrating point defects arriving at the interface cause the epitaxial regrowth of the amorphous layer.

I. INTRODUCTION

Radiation damaged layers in semiconductors are usually annealed in a furnace at temperatures in the range 500—1000 °C where solid-phase epitaxial regrowth occurs. The restoration of the crystalline structure can also be accomplished with high power laser or electron beams. These methods are mostly used to induce a fast and large temperature rise, in some cases up to temperatures where liquid-phase epitaxial regrowth occurs.

Ion-beam annealing offers a new way of restoring the crystal structure at a considerably lower temperature, 200—400 °C. The method is characterized by the use of a low-dose-rate ion beam with an energy of a few hundred keV up to some MeV. The experimental observations so far indicate that the mechanism of the ion-induced regrowth is different from the normal thermal regrowth. It is a new, interesting field for the study of radiation-induced defects and it can give valuable information on the annealing processes occurring during ion implantation at elevated temperatures.

The ion-beam-annealing phenomenon in semiconductors has been observed by several authors,[1–27] initially as an effect of the analyzing beam in Rutherford-backscattering measurements.[1–3] The phenomenon has been studied both for less heavily damaged layers[1–4,8,11,12,15,20] as well as for amorphous layers.[5,9,10,13,16,17,19–27] In some cases[1–4,15,16,20,21] a high-energy ion beam has been used. For electron beams with a sufficiently high energy, an annealing effect has also been observed.[6,7,18] Different substrate materials have been studied, such as silicon,[1–4,6,7,11–13,15–19,22,25–27] silicon on sapphire,[17,23,24] germanium,[5,8–10] indium phosphide,[20] and gallium arsenide.[6,21] A more extensive review is included in Ref. 24.

In an earlier work[24] the epitaxial regrowth of an amorphous surface layer induced by a neon beam was investigated for different parameters such as ion dose, target temperature, ion energy, and dose rate. An activation energy for the annealing mechanism was derived and a tentative model was proposed. The regrowth of a buried amorphous layer was examined in Ref. 17, while the regrowth rate was qualitatively related to the energy deposited in elastic collisions in Ref. 23.

The present investigation treats mass dependence for the ion-beam annealing of an amorphous surface layer. The purpose is to relate, quantitatively, the regrowth rate to the amount of energy deposited in elastic collisions by the annealing beam. The regrowth is studied with the Rutherford-backscattering (RBS) and channeling technique, and the initial regrowth rates are derived for the different ions. The target material was silicon on sapphire (SOS), which is an example of a thin silicon film on an insulating substrate. For very thin such layers, possibly containing shallow implantations, low-temperature annealing methods are advantageous since the diffusion of dopants and other impurities is reduced. The measurements were performed with the SOS material to enable direct comparison with earlier works, but the results also apply for bulk silicon except for minor deviations in annealing rates and/or defect structures.[17]

II. EXPERIMENTAL

A. Experimental setup

Commercially available silicon on sapphire (SOS) substrates with 1-μm-thick intrinsic (100) silicon layers were used as target material. They were cut, cleaned, and mounted on a target holder surrounded by an oven. Throughout the experiment, the target holder was placed in an ultrahigh vacuum system, operating at a pressure of 2×10^{-9} torr. The ultrahigh vacuum chamber was connected to the 400-kV accelerator at the Ion Physics Laboratory at Chalmers, Göteborg. For a description of the experimental equipment and the measurement procedure, see Ref. 24.

B. Damage production

An amorphous surface layer, ~1730 Å thick, was formed by implantation of 80-keV $^{28}Si^+$ ions to a dose of

TABLE I. Values for experimental parameters for ion annealing of a ~1600-Å-thick amorphous surface layer in 1-μm-thick SOS. (Energy: 300 keV; target temperature: 300 °C.)

Ion	Dose (cm^{-2})	Dose rate ($cm^{-2}s^{-1}$)	Direction
$^{4}He^{+}$	5.0×10^{16}–5.0×10^{17}	3×10^{13}	7° off ⟨100⟩
$^{14}N^{+}$	7.5×10^{15}–1.2×10^{17}	1×10^{13}–2×10^{13}	7° off ⟨100⟩
$^{20}Ne^{+}$	1.0×10^{16}–1.5×10^{17}	3×10^{13}	⟨100⟩
$^{28}Si^{+}$	2.5×10^{15}–6.0×10^{16}	3×10^{12}–3×10^{13}	⟨100⟩
$^{40}Ar^{+}$	2.5×10^{14}–1.0×10^{16}	1×10^{12}	⟨100⟩
$^{84}Kr^{+}$	2.5×10^{14}–1.0×10^{16}	1×10^{12}	⟨100⟩

2×10^{15} ions/cm^2 at room temperature. The target was bombarded in a direction 7° off the ⟨100⟩ axis to reduce any channeling effects, and the dose rate was 2×10^{12} ions/cm^2 s. Each bombarded area was 4 mm^2 in size, and integration of the ion current to the target was used to achieve highly accurate dose measurements.

C. Thermal annealing

The implantation was followed by three hours of thermal annealing at 300 °C. The purpose of this preheat treatment was to eliminate any thermal regrowth during the subsequent ion-beam-annealing stage. Throughout the experiment, one implanted area was left as a thermal reference which enabled a check that no further thermal annealing occurred.

D. Ion-beam annealing

Ion-beam-induced annealing of the amorphous surface layer was performed with 300-keV ions at a target temperature of 300 °C. The different ions and the beam parameters which were used are listed in Table I. The data for neon are taken from Ref. 24. The projected range (R_p) and straggling data presented in Table II have been calculated from the Lindhard-Scharff-Schiøtt (LSS) theory[28] using a computer program developed by Brice[29] and, for He^+, from the tables in Ref. 29. The irradiated area was 4 mm^2 large and the dose rate was always kept low to eliminate any beam heating. The highest dose rate used, 3×10^{13} ions/cm^2 s, corresponds to ~40 mW, which gives a negligible temperature rise.

Initial measurements showed that the dose rate is an important parameter for the regrowth, especially for the heavy ions at 300 °C where high dose rates almost inhibited the recrystallization.[30] Therefore, the dose rate was fixed at a constant low value of 1×10^{12} ions/cm^2 s for Kr^+ and Ar^+ ions in order to give comparable measurements of the annealing rates. However, for high doses of the lighter ions (with negligible dose rates dependence) a higher dose rate was used in order to avoid extremely long annealing times in which thermal effects could be important. The higher does rates for Si^+ and N^+, listed in Table I, apply only for a dose of 6×10^{16} ions/cm^2 or higher.

For Ne^+, Si^+, Ar^+, and Kr^+, where beam spreading due to multiple scattering[31] occurs within a few hundreds of Å in an amorphous layer, the annealing beam entered the target in the same direction as the proton beam used for the channeling analysis. However, for N^+ and He^+ the target was tilted 7° to reduce any channeling effects in the crystalline material below the amorphous layer.

TABLE II. Projected range R_p and straggling in amorphous silicon for the beams used for damage production and ion annealing (from Ref. 29).

Ion	Energy (keV)	Projected range (Å)	Straggling (Å)
$^{28}Si^{+}$	80	1050	410
$^{4}He^{+}$	300	17000	1900
$^{14}N^{+}$	300	7420	1460
$^{20}Ne^{+}$	300	5550	1280
$^{28}Si^{+}$	300	4080	1090
$^{40}Ar^{+}$	300	3150	930
$^{84}Kr^{+}$	300	1540	480

E. Channeling analysis

The damaged layers, as well as the ion-beam annealed layers, were analyzed by the RBS and channeling technique with 315-keV protons entering in the ⟨100⟩ direction. The backscattered particles were detected at a scattering angle of 135° with a cooled surface barrier detector. The energy resolution of the detector was ~7 keV, corresponding to a depth resolution of ~450 Å at the surface. The beam, with a divergence of less than 0.1°, was aligned with the ⟨100⟩ axis within 0.1° on a virgin crystal spot by stepping motors. They were controlled by a computerized system which also determined the alignment corresponding to the minimum of the number of backscattered particles. The probed area was 0.5 mm^2 in size, the total integrated H^+ charge for each spectrum 2.0 μC and the proton beam current typically 2 nA. The amplified pulses from the detector were passed to a multichannel analyzer and the spectra were finally stored in a computer for further data analysis.

III. RESULTS

In Fig. 1, a random backscattering spectrum for silicon together with spectra from virgin bulk silicon and virgin ~1-μm-thick silicon on sapphire are shown.[24] The drop in the yields at about 10000 Å for the SOS materials is due to the silicon/sapphire interface. A spectrum from SOS implanted with 2×10^{15} $^{28}Si^+$ ions/cm^2 at 80 keV is also included in Fig. 1, indicating that an amorphous

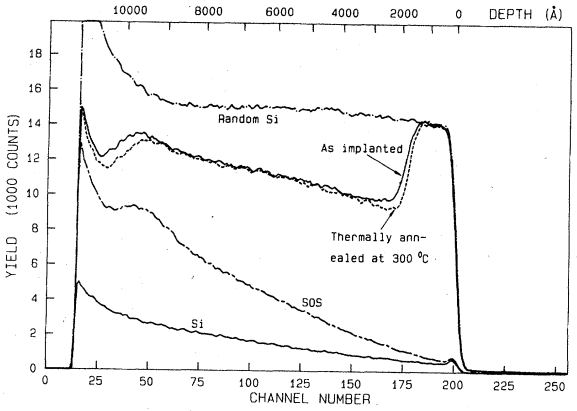

FIG. 1. Backscattering spectra for 315-keV protons channeled in the ⟨100⟩ direction in virgin (100) bulk silicon, virgin (100) silicon on sapphire (SOS), an SOS sample implanted with 2×10^{15} $^{28}Si^+$ ions/cm^2 (80 keV), and an SOS sample implanted and thermally annealed at 300 °C. A random spectrum for bulk silicon is also shown.

layer has been formed extending from the surface to a depth of ~1730 Å. The depth scale was constructed using a channeled stopping power for the incoming proton beam and a random stopping power for the backscattered particles.[32,33]

After thermal annealing at 300 °C the thickness of the amorphous layer was reduced to ~1600 Å, which was due to annealing at the heavily damaged amorphous-

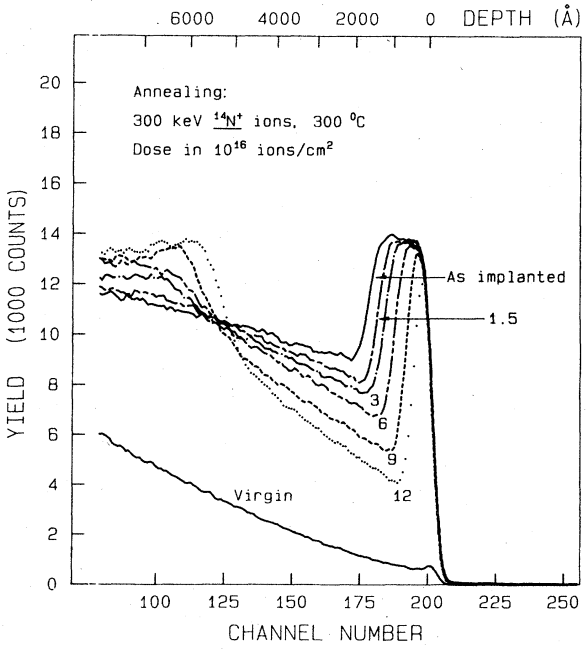

FIG. 2. Backscattering spectra (⟨100⟩ aligned) for SOS samples implanted with 2×10^{15} $^{28}Si^+$ ions/cm^2 (80 keV) and subsequently annealed with progressively higher doses of $^{14}N^+$ ions (300 keV) at 300 °C.

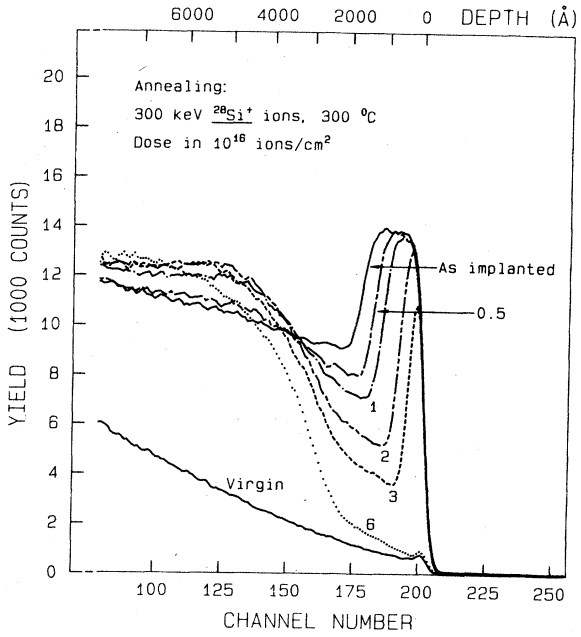

FIG. 3. Backscattering spectra (⟨100⟩ aligned) for SOS samples implanted with 2×10^{15} $^{28}Si^+$ ions/cm^2 (80 keV) and subsequently annealed with progressively higher doses of $^{28}Si^+$ ions (300 keV) at 300 °C.

crystalline transition region. As a result the interface became sharper, which can be inferred from the steeper slope of the spectrum representing the thermally annealed sample in Fig. 1. This is in agreement with electron microscopy studies by Narayan,[34] who found that during solid-phase epitaxial regrowth in (100) silicon at 450—600 °C, the amorphous-crystalline interface was atomically sharp. For continued thermal treatment at 300 °C the amorphous layer was very stable with a thermal annealing rate of at most 10 Å during each ion-beam-annealing stage (~10 h). In the succeeding figures the shown "as-implanted" spectra always refer to a sample implanted and thermally annealed.

Examples of the ion dose dependence of the annealing are presented in Figs. 2 and 3 for annealing with $^{14}N^+$ and $^{28}Si^+$ ions, respectively. The spectra are recorded following irradiation with successively higher doses. For nitrogen, a dose of 1.2×10^{17} ions/cm^2 is not sufficient to anneal completely the amorphous layer, while for silicon, less than 6×10^{16} ions/cm^2 causes a complete regrowth. The spectra show that the regrowth proceeds epitaxially from the crystalline phase towards the surface.

For all ions, an additional damage peak develops at approximately their projected range. For nitrogen the damage peak emerges at ~6000 Å. With high annealing doses the peak moves slightly towards the surface. This may be a phenomenon related to a decrease in the stopping power of the analyzing proton beam due to a larger probability for channeling as the amorphous layer is recrystallized. For silicon, the deep damage peak is located at ~4500 Å, being much broader than the nitrogen damage peak.

In Fig. 4, implanted SOS samples annealed with different ions are compared. For the heavier ions in Fig. 4(a), the dose 1×10^{16} ions/cm^2 has been chosen while a dose of 6×10^{16} ions/cm^2 has been used for the light ions in Fig. 4(b). The backscattering spectra show that a heavy ion anneals more effectively than a light ion. However, for heavier ions, the damage introduced at approximately the projected ion range (cf. Table II) is located closer to the surface and only thin crystalline surface layers can be formed. For Kr^+, the spectrum shows a tail extending to higher energies which is due to direct scattering of the protons at the implanted Kr atoms.

Annealing with He^+ ions seemed to be almost negligible. At doses higher than or equal to 2×10^{17} ions/cm^2, blistering occurred which destroyed the surface. Blistering in silicon has also been observed by other authors, e.g., with 270 keV Ar^+ ions at a dose of $\sim5\times10^{17}$ ions/cm^2.[35]

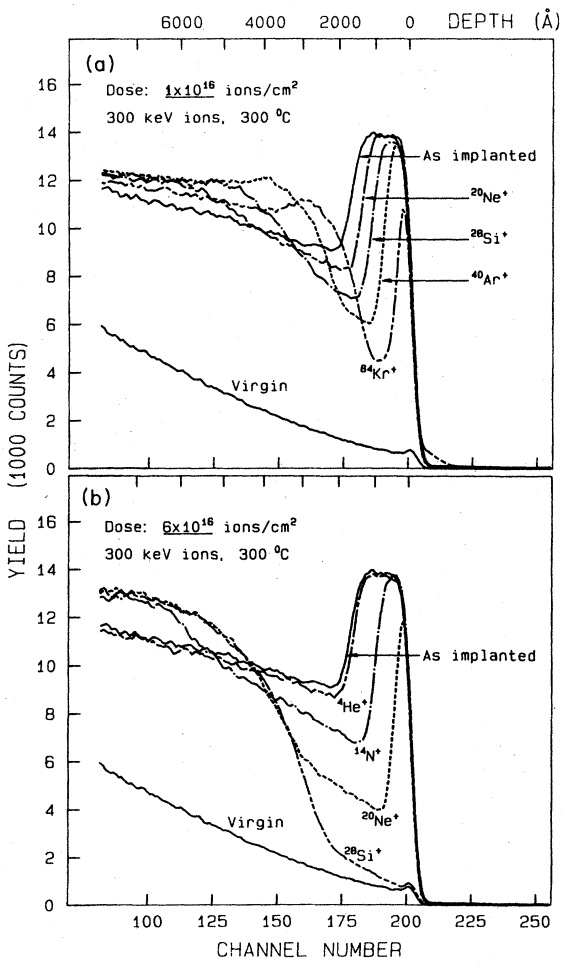

FIG. 4. Backscattering spectra (⟨100⟩ aligned) for SOS samples implanted with 2×10^{15} $^{28}Si^+$ ions/cm^2 (80 keV) and subsequently annealed with different ions (300 keV) at 300°C for a constant dose of 1×10^{16} ions/cm^2 in (a) and 6×10^{16} ions/cm^2 in (b).

IV. DATA ANALYSIS

In order to derive the annealing rate, i.e., the number of recrystallized atoms per incoming ion, it is necessary to measure the thickness of the residual amorphous layer versus ion dose very accurately. This is seriously limited by the poor resolution of the surface barrier detector. However, if it is assumed that the amorphous-crystalline interface is very narrow, which has been observed for thermal annealing,[34] the rise and fall in the backscattering spectra could be determined quite accurately, which significantly improves the thickness measurements.

Firstly, the dechanneling level was subtracted from the backscattering spectrum. This is accomplished with a computer program which calculates the dechanneled part of the incoming proton beam iteratively with depth, assuming that the ions are multiply scattered when passing through the amorphous layer. The program uses a multiple-scattering distribution derived by Sigmund and Winterbon,[31] based on a small-angle treatment of randomly distributed scattering events. For a detailed description of the method see Ref. 24. The output from the calculation is the number of scattering centers as a function of depth.

Secondly, statistical fluctuations of the defect distribution at both the rise and fall were reduced by fitting two straight lines with the method of least squares. One line was fitted to the fall at the amorphous-crystalline interface and the other to the rise at the sample surface to compensate for any drift in the absolute proton energy. From these lines, the width at half the amorphous level of the defect distribution was calculated to within ~0.3 channel numbers. This corresponds to a thickness uncertainty of ~20 Å, a more than twentyfold improvement compared to the detector resolution. The width of the remaining amorphous layer after ion annealing, in channel numbers, was then converted to a thickness in Å using a depth scale based on a random stopping power for the protons.

The advantage of the method is obvious when an amorphous layer is followed by a partially damaged layer, as for Kr^+ ion annealing, shown in Fig. 4(a). From the backscattering spectrum alone, it is difficult to extract a depth with a high accuracy since the yield behind the amorphous layer consists of the dechanneled fraction as well as protons backscattered from damage associated with the implanted Kr^+ ions.

In Fig. 5 the thicknesses of the regrown layers are plotted versus ion dose for the different ions. An annealed layer exceeding ~1560 Å represents a completely regrown layer. Complete regrowth of the amorphous layer has been obtained for all ions except for He^+, but this data is not shown in the figure since the exact dose for complete regrowth for each ion was not measured. In comparison with the annealing rate for neon published in Ref. 24, the present annealing rate appears to be slightly less. This is partly due to the subtraction of the thermal annealing effect (~100 Å) and partly to the different data analysis procedures. In the present work only the remaining amorphous layer is considered, while in Ref. 24 all defects in a constant depth interval were counted. When the thermal

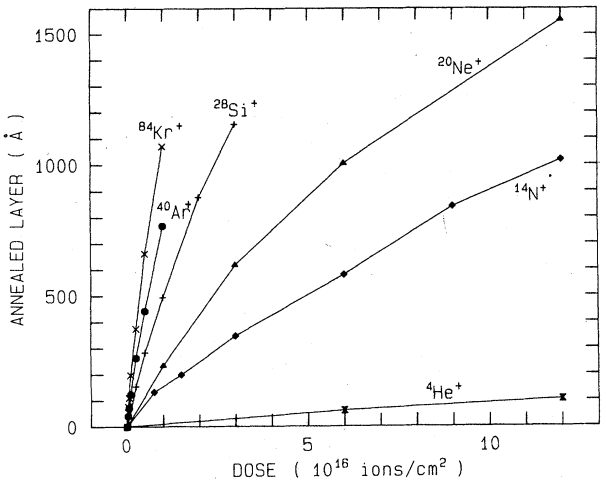

FIG. 5. Thickness of the regrown layers versus ion dose for different annealing ions.

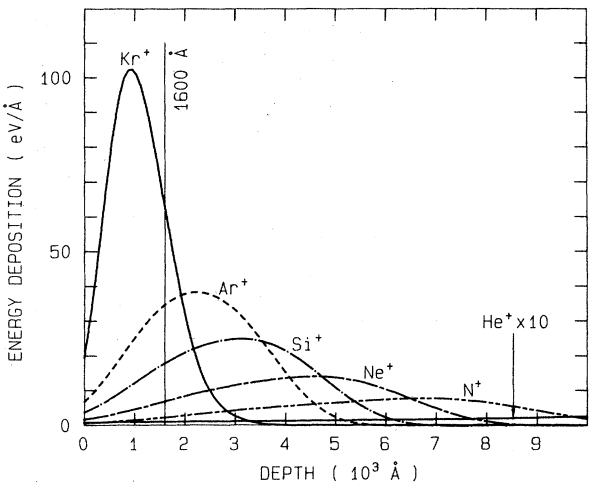

FIG. 6. Distribution of energy deposited in elastic collisions for 300-keV ions bombarding amorphous silicon.

effect is accounted for in the data in Ref. 24, the remaining discrepancy is less than 10%.

V. ENERGY DEPOSITION DISTRIBUTIONS

When an ion penetrates a solid, it loses energy due to collisions with the nuclei of the target atoms as well as in collisions with the target electrons. This is described by the nuclear and electronic stopping, respectively. If the total amount of energy deposited into atomic displacement has to be calculated, not only the incident ion but also the recoiling target atoms must be considered. Therefore, one must follow the complete collision cascade initiated by the primary ion. The scattering of ions or atoms with target nuclei is described by the LSS theory[28] and the frictional force of electronic stopping is treated by Lindhard and Scharff.[36] The depth distribution emanating from such calculations is called the nuclear (elastic) energy deposition distribution or damage distribution. The corresponding distribution of the energy deposited into electronic processes is usually labeled the ionization distribution.

It should be noted that the nuclear energy deposition distribution represents the initial collision cascade which develops during a time of the order of $\sim 10^{-12}$ s and which is essentially temperature independent. The amount of damage remaining after a macroscopic time is, however, dependent on whether the produced defects are frozen in or if they are able to migrate.

Winterbon[37] has derived both the damage and ionization distributions by solving linear Boltzmann transport equations describing the collision cascade. Interpolation of the moments in Ref. 37 to the proper ion-target combination was used to construct a fourth-order Edgeworth expansion of the distribution of energy deposited in nuclear collisions, Fig. 6. The He^+ curve is taken from the high-energy distributions of Brice[29] and has been multiplied by a factor of 10. The position of the initial amorphous-crystalline interface is shown by the vertical line at 1600 Å. Apparently, the energy deposited into atomic motion within the initial amorphous layer, as well as at the interface, increases with ion mass.

To relate the annealing rate to the energy deposited in elastic collisions, the derivative of the regrown layer thickness with respect to ion dose was calculated at zero dose. This represents the initial annealing rate which would not be influenced by any implanted ions or damage caused by the annealing beam. The initial annealing rate, expressed as the number of annealed Å for a dose of 1×10^{15} ions/cm^2, is plotted versus the elastic energy deposition at 1600 Å in Fig. 7. By multiplication with the atomic density for silicon, the annealing rate is also expressed as the number of "recrystallized atoms" per incoming ion. The straight line shown has been fitted to the points by the method of least squares. The accuracy of the derived annealing rate is limited by the differentiation, giving an error which is estimated to be less than 20%.

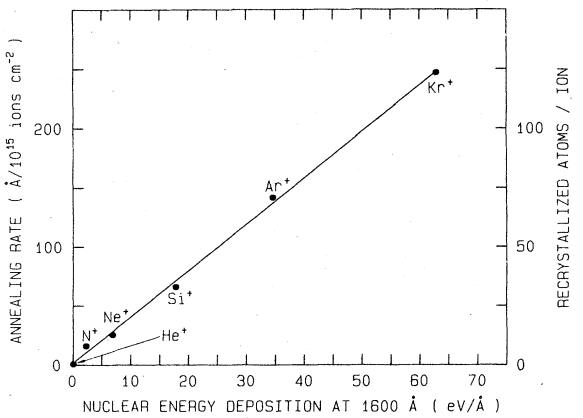

FIG. 7. Initial annealing rate, i.e., the thickness of the recrystallized layer per ion dose at zero dose, versus the amount of nuclear energy deposition at a depth of 1600 Å.

VI. DISCUSSION

A. Annealing rate and damage production for the annealing ion beam

According to Fig. 7, the initial annealing rate is proportional to the amount of energy which goes into elastic collisions at the amorphous-crystalline interface, i.e., the intersection of the initially produced collision cascade with the interface. This relationship seems to explain the measured large differences in annealing rates for the different ions (more than 2 orders of magnitude). The electronic energy loss for all the studied ions[36] are, however, of approximately the same magnitude and, therefore, cannot account for the differences in annealing rates. These conclusions are also supported by the measured energy dependence of the ion-beam annealing.[12,23–25] However, due to a significant dose rate dependence,[30] the proportional constant between the annealing rate and the nuclear energy deposition represents a specific dose rate (1×10^{12} ions/cm^2 s). At higher dose rates, large deviations from this linear dependence will occur, especially for heavy ions, while only minor deviations are expected for lower dose rates.

The annealing rate, as can be seen from Fig. 5, is highest at a depth 1600 Å, where the regrowth begins, and decreases as the regrowth proceeds towards the surface. Except for Kr^+ ions, the nuclear energy deposition shows the same depth dependence, Fig. 6, giving further support for the proportionality found. If the annealing rate is taken from the data in Fig. 5 at different depths, i.e., when the regrowth has proceeded a specific distance (<1000 Å), and plotted versus the appropriate amount of energy deposition in Fig. 7, the new points will indeed follow the straight line, at least for N^+, Ne^+, and Si^+. However, for the heavier ions, deviations will be found, which increase with ion mass. Starting with about 15% lower annealing rate for Si^+ ions, which is still within the accuracy of the differentiation method, the annealing rate for Kr^+ ions is reduced to less than half that obtained at the depth 1600 Å. The explanation is probably that, for a given energy, the implanted ions and the damage they produce are located closer to the surface, the heavier the ion mass. For instance, the damage peak at ~2300 Å created by the Kr^+ ions [see Fig. 4(a)], extends all the way to the amorphous-crystalline interface at ~500 Å and the implanted Kr ions even extend to the surface. This effect of implanted ions and the damage they introduce, since the phenomenon occurs for Si^+ ions as well, probably reduces the regrowth rate.

The damage peak associated with the annealing ions which develops below the amorphous layer, see Figs. 2—4, appears to be positioned at the projected ion range rather than at the calculated damage depth. For Ar^+, Si^+, and Ne^+ ions of 300 keV as well as for Ne^+ ions of 100 and 200 keV,[23] this damage peak coincides with the peak of the projected ion range distribution within 400 Å. For Kr^+ ions, the peak is positioned even beyond the peak of the projected range distribution (~800 Å), in agreement with Ref 13, while for N^+ the peak is shifted ~2000 Å towards the surface (i.e., shallower than the calculated damage distribution). The absolute calculated depths for the projected range and damage distributions depend, however, on the electronic stopping from the LSS theory[36] which does not account for effects of the electronic shells for different ions.

The shift of the damage peak towards or beyond R_p from the depth given by Winterbon[37] for low-temperature implantation, has been observed by several authors[13,38,39] when the implantation temperature is raised. Some alterations of the damage distributions would be expected since defects are highly mobile at 300 °C which, e.g., increases the probability for annihilation. The high-temperature damage peak has also been shown to be accompanied by a higher dechanneling rate[38] which can be perceived in the defect distributions calculated from the backscattering spectra in the present work. This suggests the formation of different types of defects during high-temperature implantation as opposed to implantations at room temperature or below. There are some indications from electron microscopy studies[25,40] that these defects are extended defects consisting of defect clusters and dislocation loops. The explanation could be that point defects, generated by the annealing beam in proportion to the amount of energy deposited in elastic collisions, become mobile due to the elevated temperature. Instead of being frozen along the damage distribution, these point defects diffuse randomly, and when they encounter an implanted atom or a defect center they could become trapped, eventually forming an extended defect.

B. Comparison with a model for ion-beam annealing

The ion mass dependence for the ion-beam-induced regrowth gives further support for the annealing model described in Ref. 24. The model assumes that vacancies and interstitials are generated by the irradiating beam and due to the elevated temperature they become mobile. The amorphous-crystalline interface acts as a sink for these migrating point defects. Arriving at the interface, they contribute to recrystallization. An activation energy of ~0.36 eV was found for the migration process.

The proportionality between the annealing rate and the nuclear energy deposition clearly strengthen the first assumption in the model, i.e., that the rate of regrowth is proportional to the production rate of point defects. It is further concluded that the complete collision cascade initiated by the primary ion is responsible for the generation of such defects. This enables a large number of them to be created in the vicinity of the amorphous-crystalline interface and therefore accounts for the observed large number of "recrystallized atoms" for each ion, see Fig. 7.

The proportional constant from Fig. 7 is ~2 recrystallized atoms per eV/Å of nuclear energy deposition for each ion. Assuming that the positioning of one atom at a crystal lattice site is the result of one vacancy arriving at the interface, and if an energy of 20 eV is required for the creation of a vacancy-interstitial pair, then 40 eV must be provided for the regrowth of 2 atoms. If it is further assumed that all vacancies created by the ion beam within a certain distance of the interface participate in the recrystallization process, then an ion having an energy deposition of 1 eV/Å must penetrate a distance of 40 Å for the

regrowth of 2 atoms. If recombination processes are considered, this diffusion distance will probably increase somewhat. Interstitials are also assumed to participate in the regrowth, but due to their higher migration velocity, vacancy migration would be the limiting step for the annealing process. The detailed mechanism on an atomic scale is not yet known but the simple estimation of the migration distance for the vacancies may justify the fact that the nuclear energy deposition in Fig. 7 was taken at the specific depth of 1600 Å without integrating over, maybe, thousands of Å. We speculate that the increased regrowth rate with increased temperature[24] is due to a longer such diffusion distance for the point defects.

From the mass and energy dependence of the ion-beam annealing it seems favorable to use a high mass ion with a low energy to achieve the highest annealing rate. However, the damage introduced at $\geq R_p$ is probably a serious problem for the quality of the recrystallized layer. The dose rate dependence for heavy ions would also require long annealing times. Thus, the conclusion is that in order to produce more defect-free regrown layers, a low mass ion or a high energy is preferable at the expense of a high dose.

VII. SUMMARY

The epitaxial regrowth of a 1600-Å-thick amorphous surface layer in silicon at 300 °C due to low-intensity irradiation of a 300-keV ion beam has been measured for different ions. The initial regrowth rate has been shown to be proportional to the amount of energy deposited in elastic collisions at the amorphous-crystalline interface. However, the annealing ions produce damage at about their projected range, which limits the width and the crystallinity of the annealed layer. The experimental data favor a model relying on the migration of point defects, created by the ion beam, to the amorphous-crystalline interface where they contribute to the recrystallization.

ACKNOWLEDGMENTS

The authors are indebted to J. Jacobsson and A. Kangasmaa for technical assistance and D. K. Brice for kindly sending us his computer program. Discussions with W. L. Brown, R. G. Elliman, J. S. Williams, and P. Sigmund are gratefully acknowledged. The work was financially supported by the Swedish Board for Technical Development and the Swedish Natural Science Research Council.

---

*Permanent address: National Defense Research Institute, Department 3, S-581 11 Linköping, Sweden.

[1]J. E. Westmoreland, J. W. Mayer, F. H. Eisen, and B. Welch, Radiat. Eff. **6**, 161 (1970).

[2]E. Bøgh, P. Høgild, and I. Stensgaard, Radiat. Eff. **7**, 115 (1971).

[3]J. K. Hirvonen, W. L. Brown, and P. M. Glotin, in *Proceedings of the Second International Conference on Ion Implantation in Semiconductors, Garmisch-Partenkirchen,* edited by I. Ruge and J. Graul (Springer, Berlin, 1971), p. 8.

[4]S. T. Picraux and F. L. Vook, Radiat. Eff. **11**, 179 (1971).

[5]G. Holmén and P. Högberg, Radiat. Eff. **12**, 77 (1972).

[6]N. N. Gerasimenko, A. V. Dvurechenskii, G. A. Kachurin, N. B. Pridachin, and L. S. Smirnov, Fiz. Tekh. Poluprovodn. **6**, 1834 (1972) [Sov. Phys.—Semicond. **6**, 1588 (1973)].

[7]M. D. Matthews and S. J. Ashby, Philos. Mag. **27**, 1313 (1973).

[8]G. Holmén, P. Högberg, and A. Burén, Radiat. Eff. **24**, 39 (1975).

[9]G. Holmén, S. Peterström, A. Burén, and E. Bøgh, Radiat. Eff. **24**, 45 (1975).

[10]G. Holmén, A. Burén, and P. Högberg, Radiat. Eff. **24**, 51 (1975).

[11]H. E. Roosendaal, W. H. Kool, and F. W. Saris, Radiat. Eff. **36**, 35 (1978).

[12]W. H. Kool, H. E. Roosendaal, L. W. Wiggers, and F. W. Saris, Radiat. Eff. **36**, 41 (1978).

[13]I. Golecki, G. E. Chapman, S. S. Lau, B. Y. Tsaur, and J. W. Mayer, Phys. Lett. **71A**, 267 (1979).

[14]G. A. Kachurin, Fiz. Tekh. Poluprovodn. **14**, 787 (1980). [Sov. Phys.—Semicond. **14**, 461 (1980)].

[15]J. Nakata, M. Takahashi, and K. Kajiyama, Jpn. J. Appl. Phys. **20**, 2211 (1981).

[16]J. Nakata and K. Kajiyama, Appl. Phys. Lett. **40**, 686 (1982).

[17]B. Svensson, J. Linnros, and G. Holmén, Nucl. Instrum. Methods **209/210**, 755 (1983).

[18]J. Washburn, C. S. Murty, D. Sadana, P. Byrne, R. Gronsky, N. Cheung, and R. Kilaas, Nucl. Instrum. Methods **209/210**, 345 (1983).

[19]D. K. Sadana, J. Washburn, P. F. Byrne, and N. W. Cheung, in *Materials Research Society Symposium Proceedings 14,* edited by S. Mahajan and J. W. Corbett (North-Holland, New York, 1983), p. 511.

[20]Zhang Tong He and G. Carter, Radiat. Eff. **77**, 97 (1983).

[21]D. K. Sadana, H. Choksi, J. Washburn, P. F. Byrne, and N. W. Cheung, Appl. Phys. Lett. **44**, 301 (1984).

[22]O. W. Holland and J. Narayan, Appl. Phys. Lett. **44**, 758 (1984).

[23]G. Holmén, J. Linnros, and B. Svensson, Appl. Phys. Lett. **45**, 1116 (1984).

[24]J. Linnros, B. Svensson, and G. Holmén, Phys. Rev. B **30**, 3629 (1984).

[25]R. G. Elliman, S. T. Johnson, A. P. Pogany, and J. S. Williams, Proceedings of the Conference on Ion Beam Modification of Materials—IBMM 84, Ithaca, 1984 (unpublished).

[26]R. G. Elliman, S. T. Johnson, K. T. Short, and J. S. Williams, *Materials Research Society Symposium Proceedings 27,* edited by G. K. Hubler, O. W. Holland, C. R. Clayton, and C. W. White (North-Holland, New York, 1984), p. 229.

[27]K. T. Short, D. J. Chivers, R. G. Elliman, J. Liu, A. P. Pogany, H. Wagenfeld, and J. S. Williams, *Materials Research Society Symposium Proceedings 27,* edited by G. K. Hubler, O. W. Holland, C. R. Clayton, and C. W. White (North-Holland, New York, 1984), p. 247.

[28]J. Lindhard, M. Scharff, and H. E. Schiøtt, Mat. Fys. Medd. Dan. Vid Selsk. **33**, 14 (1963).

[29]D. K. Brice, Sandia Laboratories Research Report No. SAND-75-0622, July, 1977 (unpublished); D. K. Brice, *Ion Implantation Range and Energy Deposition Distributions* (Plenum, New York, 1975), Vol. 1.

[30]J. Linnros and G. Holmén (unpublished).

[31]P. Sigmund and K. B. Winterbon, Nucl. Instrum. Methods **119**, 541 (1974).
[32]F. Cembali and F. Zignani, Radiat. Eff. **31**, 169 (1977).
[33]H. H. Andersen and J. F. Ziegler, in *Hydrogen Stopping Powers and Ranges in all Elements,* edited by J. F. Ziegler (Pergamon, New York, 1977), Vol. 3.
[34]J. Narayan, J. Appl. Phys. **53**, 8607 (1982).
[35]K. Wittmaack and W. Wach, Appl. Phys. Lett. **32**, 532 (1978).
[36]J. Lindhard and M. Scharff, Phys. Rev. **124**, 128 (1961).
[37]K. B. Winterbon, *Ion Implantation Range and Energy Deposition Distributions* (Plenum, New York, 1975), Vol. 2.
[38]L. Csepregi, E. F. Kennedy, S. S. Lau, J. W. Mayer, and T. W. Sigmon, Appl. Phys. Lett. **29**, 645 (1976).
[39]D. K. Sadana, M. Stratham, J. Washburn, and G. R. Booker, J. Appl. Phys. **51**, 5718 (1980).
[40]L. D. Glowinski, K. N. Tu, and P. S. Ho, Appl. Phys. Lett. **28**, 312 (1976).